Identification of the ferroxidase centre of *Escherichia coli* bacterioferritin

Nick E. LE BRUN,* Simon C. ANDREWS,† John R. GUEST,† Pauline M. HARRISON,† Geoffrey R. MOORE* and Andrew J. THOMSON*‡

*Centre for Metalloprotein Spectroscopy and Biology, School of Chemical Sciences, University of East Anglia, Norwich NR4 7TJ, and †The Krebs Institute, Department of Molecular Biology and Biotechnology, University of Sheffield, Sheffield S10 2TN, U.K.

The bacterioferritin (BFR) of *Escherichia coli* takes up iron in the ferrous form and stores it within its central cavity as a hydrated ferric oxide mineral. The mechanism by which oxidation of iron (II) occurs in BFR is largely unknown, but previous studies indicated that there is ferroxidase activity associated with a site capable of forming a dinuclear-iron centre within each subunit [Le Brun, Wilson, Andrews, Harrison, Guest, Thomson and Moore (1993) FEBS Lett. **333**, 197–202]. We now report site-directed mutagenesis experiments based on a putative dinuclear-metal-ion-binding site located within the BFR subunit. The data reveal that this dinuclear-iron centre is located at a site within the four-α-helical bundle of each subunit of BFR, thus identified as the ferroxidase centre of BFR. The metal-bound form of the centre bears a remarkable similarity to the dinuclear-iron sites of the hydroxylase subunit of methane mono-oxygenase and the R2 subunit of ribonucleotide reductase. Details of how the dinuclear centre of BFR is involved in the oxidation mechanism were investigated by studying the inhibition of iron (II) oxidation by zinc (II) ions. Data indicate that zinc (II) ions bind at the ferroxidase centre of apo-BFR in preference to iron (II), resulting in a dramatic reduction in the rate of oxidation. The mechanism of iron (II) oxidation is discussed in the light of this and previous work.

INTRODUCTION

Bacterioferritin (BFR) of *Escherichia coli* is an iron-storage protein consisting of 24 identical subunits (18.5 kDa) that pack together to form a highly symmetrical, approximately spherical protein shell surrounding a central 8 nm cavity, in which large amounts of iron can be stored. Six 4-fold and eight 3-fold hydrophilic channels connect the inner core with the protein environment. The *bfr* gene of *E. coli* has been cloned, sequenced and overexpressed to yield BFR as 15% of soluble cell protein [1,2]. Secondary structure prediction, molecular modelling and, most recently, X-ray crystallographic studies have revealed a close structural similarity between BFR and the ferritins, a family of iron-storage proteins found in both eukaryotic and prokaryotic cells [3–10]. The conservation of key residues within the ferritins and BFRs indicates a distant evolutionary relationship between them [4,6,7]. However, a major difference between the two is that BFR contains up to 12 *b*-type haem groups, while ferritins, as isolated, do not contain haem. The haem groups, bound by two methionine residues [11], are located at inter-subunit sites [9,12].

Common to both ferritins and BFRs is a capacity to store large quantities of iron, within their hollow interior, in the form of an hydrated ferric oxide mineral containing variable amounts of phosphate anion [3,13,14]. Core reconstitution studies show that iron can be taken up by the iron-free (apo-) protein as iron (II) and oxidized to iron (III) during a process catalysed by the protein coat [15–21]. This is termed the ferroxidase activity.

However, it is beginning to emerge from studies of different ferritins that there may be several different routes of iron (II) oxidation capable of leading to core deposition. Eukaryotic ferritins are composed of two subunits known as H- and L-chains that differ in their primary sequence and in the rate at which they catalyse iron (II) oxidation. Recombinant ferritin composed only of H-chain shows a rapid oxidation process [17,18,22,23] that, in bullfrog ferritin, saturates at two iron (II) ions per subunit [24], whereas the L-chain-only ferritin shows a much decreased rate of iron oxidation. However, both H- and L-chain ferritins are capable of forming an iron core [24,25].

X-ray crystallographic studies of H-chain ferritin revealed a metal-binding site, occupied by terbium (III) or calcium (II) in the crystal structure, which was assumed to be capable of binding iron [26]. A study of the effects of site-directed mutagenesis on iron (II) uptake gave support to the proposal that iron oxidation can take place at a dinuclear-iron centre, and a model in which a μ-oxo bridged iron (III) dimer is formed at this centre, termed the ferroxidase centre, has been proposed [18,19,23,27].

In previous studies of iron uptake by apo-BFR, iron incorporation was shown to consist of at least three kinetically distinguishable phases, termed, in order of occurrence, phases 1, 2 and 3 [21]. Phase 1, detected by the stopped-flow measurement of a fast, < 1 nm blue-shift perturbation of the haem group Soret absorption band, was assigned to the binding of iron (II) by the protein. Phase 2, measured in a stopped-flow spectrophotometer at 340 nm, was found to saturate at a level of two iron (II) ions per subunit and was attributed to the oxidation of two iron (II) to iron (III) ions per subunit. This stoichiometry is consistent with the idea that a dinuclear-iron (II) centre is the site of dioxygen reaction. Phase 3, also measured at 340 nm, was observed only when the ratio of added iron to protein exceeded 50, and was assigned to the subsequent, relatively slow formation of an iron core.

Molecular modelling of BFR, based on the structure of H-chain ferritin, identified two potential iron-binding sites [8]. One was a putative dinuclear centre positioned within the four-α-helical bundle of the subunit, while the other was a mononuclear site located within the hydrophilic 3-fold channels of the protein. A dinuclear site was also proposed in *A. vinelandii* BFR by Grossman et al. [7] based on a sequence alignment with human H-chain ferritin. On the basis of our previous kinetic work, the putative dinuclear-iron centre was proposed to be the iron-bound form of the ferroxidase centre of BFR [21]. While our

Abbreviations used: BFR, bacterioferritin; MMO, methane mono-oxygenase; RNR, ribonucleotide reductase.

‡ To whom correspondence should be addressed.

work was in progress, an X-ray structure of *E. coli* apo-BFR was reported by Frolow et al. [9]. This structure does indeed reveal that metal ions bind at a dinuclear site within the protein that is similar to the proposed site in our earlier modelling study. Here, we report the results of a programme of mutagenesis experiments designed to test the proposal that the dinuclear centre is important in the iron-uptake mechanism of BFR.

Four site-directed variants of BFR have been generated, in which residues proposed to be involved in iron ligation at the two putative metal-binding sites have been replaced by non-complexing residues. Three dinuclear-iron site variants were investigated: $E^{18} \rightarrow A$ and $E^{94} \rightarrow A$, which contain a substitution in the co-ordination sphere of each of the metal ions of the dimer; and $E^{51} \rightarrow A$, which contains the substitution of a single residue that is proposed to bridge the two metal ions. One 3-fold channel variant, $D^{118} \rightarrow A$, was investigated. The kinetic characterization of the variants together with studies of the interaction of zinc (II) ions with BFR show that the dinuclear site proposed by Cheesman et al. [8], and confirmed to be present by Frolow et al. [9], is central to the rapid oxidation of iron (II) in BFR.

EXPERIMENTAL

Site-directed mutagenesis

Site-directed mutagenesis was performed by the single-primer method [28]. The mutagenesis target was a single-stranded M13mp18 derivative containing the 4.9 kb *Eco*RI–*Hin*dIII *bfr* fragment from the plasmid pGS280 [2]. The post-mutagenesis progeny phage were screened for the desired mutations by nucleotide sequence analysis [29] of purified single-stranded DNA [30]. Four mismatch mutagenic primers were used to direct the following substitutions (binding coordinates from Andrews et al. [2]): S271, $E^{18} \rightarrow A$ [5′-d(G GGA AAT G*C*G CTT GTC)-3′; 555–570]; S272, $D^{118} \rightarrow A$ [5′-d(C AGC CGC G*C*T ATG ATG ATA GAA)-3′; 855–876]; S273, $E^{51} \rightarrow A$ [5′-d(C ATT GAT G*C*G ATG AAA CAC)-3′; 654–672]; and S274, $E^{94} \rightarrow A$ [5′-d(G GCA CTT G*C*G CTG GAT G)-3′; 783–799].

The nucleotide sequences of the primers are identical to the corresponding *bfr* sequence except for the mismatches (in italic) designed to direct the amino acid substitutions. The complete *bfr* nucleotide sequence of each identified mutant was determined and verified. Double-stranded replicative form DNA was prepared for each verified mutant, and the 1.2 kb *Eco*RI–*Pst*I *bfr*-fragment was subcloned into the corresponding sites of pUC119. The mutated *bfr* genes were expressed from the natural *bfr* promoter [31].

Overproduction and purification of BFR and BFR variants

Phagemid pUC119 derivatives carrying the mutated *bfr* genes were used to transform strain JRG2157, a Δ*bfr*::*kan* derivative of JM101 (*thi*, *supE*, Δ*proAB-lac/F' traD36*, *proA*$^+$*B*$^+$, *lacI*^{q}*Z*ΔM15) [32], which provides a source free of wild-type BFR for the overproduction of BFR variants. The resultant overproducing strains were grown aerobically for 16 h at 37 °C in L broth containing 150 μg/ml ampicillin. BFR variants were purified using the method described previously [31] with the following modifications: buffer C [20 mM Hepes (pH 7.8)/100 mM KCl/0.1 mM EDTA/10% glycerol] was used in place of phosphate-buffered saline (buffer A; pH 7.2) and anion-exchange chromatography was performed with a Protein-PakQ (20 mm × 100 mm) column from Waters (in place of the Q-Sepharose column) equilibrated with buffer C and eluted at 2.5 ml/min with a 300 ml linear gradient of 0.0–0.1 M $(NH_4)_2SO_4$ in buffer C.

Iron and protein assay

Iron was assayed by the method of Drysdale and Munro [33] with 1% ferrozine in place of 0.5% 2,2′-bipyridyl. Protein was measured using the bicinchoninic acid assay [34], employing BSA as a standard. Haem was determined using the pyridine haemochromogen method of Falk [35].

Iron removal from BFR and BFR variants

Non-haem iron was removed from BFR and variants by reduction with sodium dithionite, as described previously [18].

Spectroscopic detection of haem and non-haem iron species

Haem iron is readily distinguished from non-haem iron by most spectroscopies, particularly UV–visible spectrophotometry and EPR. The distinction between different forms of non-haem iron species is less straightforward. Monomeric high-spin iron (II) is an even-spin system that is undetectable by conventional EPR and does not have a strong colour, so it is generally not detectable by visible spectrophotometry. We have used NO as an EPR spin probe to form iron (II)–NO adducts in BFR that are EPR detectable [36]. Monomeric high-spin iron (III) is both EPR detectable and has a colour, so it is detectable by visible spectrophotometry. The EPR characteristics of iron (III), dinuclear iron (III) and mixed valence iron (II)–iron (III) species are different, leading to simple differentiation between them. However, all species containing iron (III) ligated by oxygen atoms possess broad absorbance in the near-UV–visible region, so measurement of the rate of increase at a wavelength in this region only follows the rate of iron (II) oxidation and does not distinguish between products.

Kinetic measurements of changes in absorption after the addition of iron (II) (freshly prepared prior to each experiment by dissolving weighed amounts of ferrous ammonium sulphate in de-oxygenated AnalaR-grade water) or zinc (II) ions to wild-type apo-BFR and apo-BFR variants were made using either a conventional UV–visible spectrophotometer (Aminco DW2000, Hitachi U4001 or Hitachi U3200), for which additions to the sample were made using a micro-syringe (Hamilton) or by using a stopped-flow apparatus (Applied Photophysics DX17MV) with the BFR solution in one syringe and the metal-ion solution in another. Changes in the haem absorbance were monitored in the 405–425 nm region of the spectrum [21], while the oxidation of iron (II) to iron (III) was monitored at 340 nm.

EPR spectra were measured with an X-band spectrometer (Bruker ER200D with an ESP 1600 computer system) fitted with a liquid helium flow cryostat (Oxford Instruments plc; ESR9).

RESULTS AND DISCUSSION

Construction, overproduction and purification of BFR variants

Mutagenic primers, containing mismatches designed to generate the desired missense mutations, were used to mutagenize the cloned *bfr* gene. Nucleotide sequence analysis of 59 potential mutants identified five valid mutants representing the four desired mutations. The 1.2 kb *Eco*RI–*Pst*I fragments, containing the mutated *bfr* genes, were subcloned into pUC119, generating the following plasmids (with the indicated missense mutations): pGS730 ($E^{18} \rightarrow A$), pGS731 ($E^{51} \rightarrow A$), pGS733 ($E^{94} \rightarrow A$) and pGS734 ($D^{118} \rightarrow A$). The mutated *bfr* genes were then over-expressed in transformants of the BFR-free strain, JRG2157, to avoid contamination with wild-type BFR. The overproducing strains were grown to late stationary phase and harvested. The overproduced BFR variants and wild-type BFR were purified,

Table 1 Haem and non-haem iron contents of BFR and its variants as isolated

Haem and non-haem iron contents were determined using the methods described in the Experimental section.

Sample	Haem per 24-mer	Non-haem iron per 24-mer
Wild-type BFR	~ 5–6	~ 28
$E^{18} \rightarrow A$ BFR (dinuclear-iron site variant)	~ 8–9	~ 6
$E^{51} \rightarrow A$ BFR (dinuclear-iron site variant)	~ 11–12	~ 12
$E^{94} \rightarrow A$ BFR (dinuclear-iron site variant)	~ 8–9	~ 9
$D^{118} \rightarrow A$ BFR (3-fold channel variant)	~ 4–5	~ 100

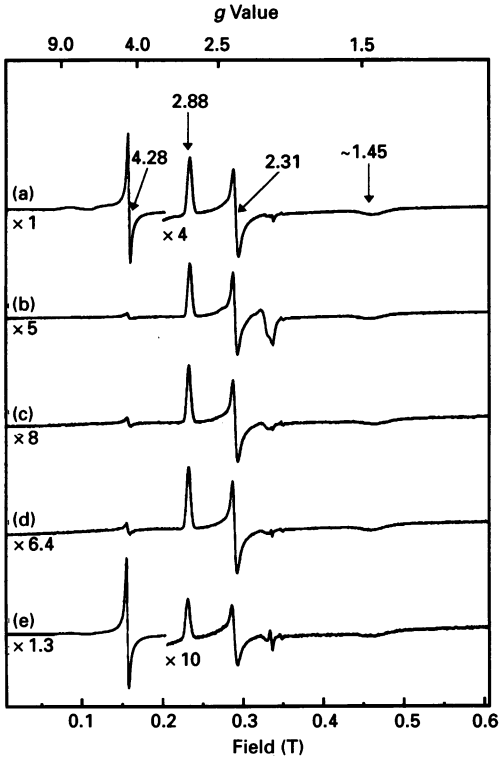

Figure 1 X-band EPR spectra of wild-type BFR and its variants in 20 mM Hepes buffer/10% (v/v) glycerol/100 μM EDTA, pH 7.8

(**a**) Wild-type BFR (60 μM); (**b**) $E^{18} \rightarrow A$ BFR (34 μM); (**c**) $E^{51} \rightarrow A$ BFR (16 μM); (**d**) $E^{94} \rightarrow A$ BFR (23 μM); and (**e**) $D^{118} \rightarrow A$ BFR (21 μM). Conditions: microwave frequency 9.39 GHz; microwave power 2.01 mV; modulation amplitude 1 mT; temperature 10 K.

and the BFR variants were found to resemble the wild-type protein in eluting as 500 kDa proteins from a gel permeation column and in being heat stable (65 °C for 15 min).

Initial characterization of wild-type BFR and BFR variants

Determinations of the haem and non-haem iron contents of BFR and its variants are given in Table 1. In previous studies, the haem content of over-produced wild-type BFR has been observed

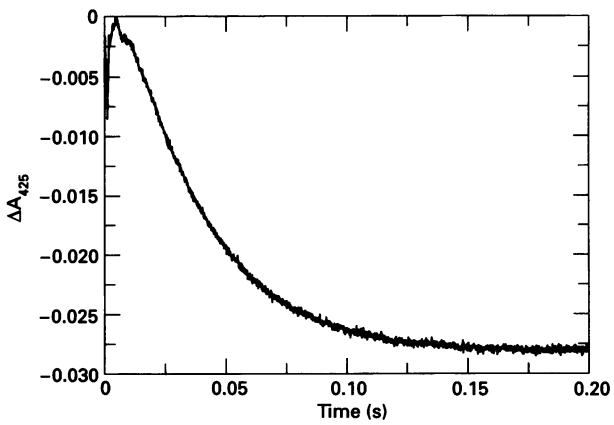

Figure 2 Phase 1 of iron uptake by wild-type apo-BFR

Absorption change at 425 nm measured by the stopped-flow method as a function of time after the addition of 100 iron (II) ions per wild-type apo-BFR molecule. The protein (concentration after mixing, 2.25 μM) was in 100 mM Mes buffer, pH 6.5 at 30 °C. Pathlength was 1 cm.

to vary widely [8], and a spread of haem loadings is also observed here. The non-haem iron content of over-produced BFR, as isolated, is usually less than 100 irons per molecule [8], compared with approx. 1000 irons per molecule in BFR from non-overexpressing *E. coli* [37]. Low iron loadings in over-produced BFR may be due to the abundance of BFR in the cell. An extremely low level of non-haem iron is observed in each of the three dinuclear-iron site variants, while the iron content of the 3-fold channel variant is approx. three times that of wild-type BFR. Differences between the variants may reflect altered properties of the proteins, but extensive investigation of the physiology of the over-producing cells would be required to test this.

The 10 K EPR spectra of wild-type BFR and the BFR variants (Figures 1a–1e), confirm the distribution of iron given in Table 1. Taking into account the differences in concentration of the protein samples, it can be seen that the signal at $g = 4.28$, due to mononuclear, high-spin $S = 5/2$ iron (III), is of highest intensity in the 3-fold channel variant, $D^{118} \rightarrow A$ BFR. The $g = 4.28$ signal of wild-type BFR is approx. one third the intensity of that of $D^{118} \rightarrow A$ BFR and is present in each of the dinuclear-iron site variants with a very low intensity similar to that usually assigned to adventitious binding of iron (III). Signals at $g = 2.88$, 2.31 and ~ 1.45 in the spectrum of Figure 1(a) are due to the low-spin $S = 1/2$ haem groups of wild-type BFR. The haem g values in the spectra of the BFR variants (Figures 1b–1e) are identical to those of wild-type BFR, indicating that these single amino acid substitutions have not significantly affected the haem environment.

Kinetic analysis of iron uptake by wild-type apo-BFR and apo-BFR variants

Phase 1 of the iron-uptake process by wild-type apo-BFR and its variants was investigated by adding ferrous ammonium sulphate to aerobic solutions of the apo-protein samples and by monitoring changes in absorption at 425 nm as a function of time. One representative measurement at 425 nm, after the addition of 100 iron (II) ions per wild-type apo-BFR molecule at 20 °C, is shown in Figure 2.

Wild-type apo-BFR exhibited a maximum decrease of approx. 0.025 absorption units at 425 nm, in agreement with

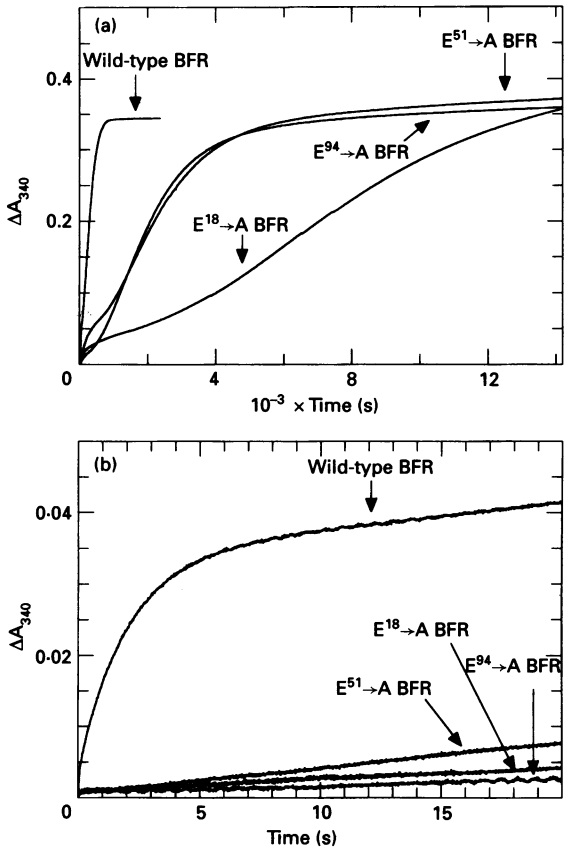

Figure 3 Phases 2 and 3 of iron uptake by wild-type apo-BFR and $E^{18} \rightarrow A$, $E^{51} \rightarrow A$ and $E^{94} \rightarrow A$ apo-BFR variants

(**a**) Absorption change at 340 nm measured as a function of time after the addition of 400 iron (II) ions per apo-protein molecule. Proteins were in 100 mM Mes buffer, pH 6.5, at a concentration of 0.5 μM. Temperature was 30 °C, pathlength 1 cm. (**b**) Absorption change at 340 nm followed by spectrophotometry over the first 20 s after the addition of 400 iron (II) ions per apo-protein molecule. Proteins were in 100 mM Mes buffer, pH 6.5, to give a concentration after mixing of 0.5 μM. Temperature was 30 °C, pathlength 1 cm.

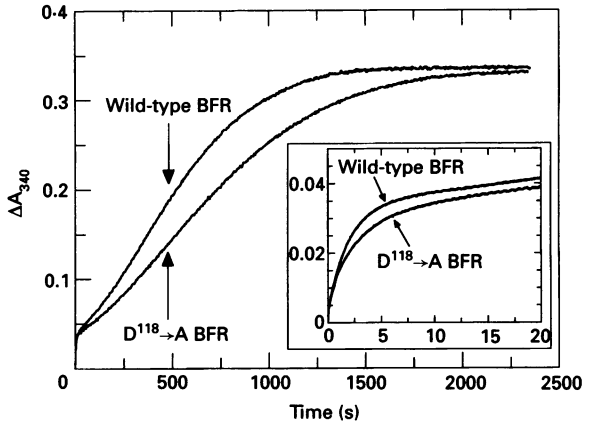

Figure 4 Phases 2 and 3 of iron uptake by wild-type apo-BFR and 3-fold channel variant $D^{118} \rightarrow A$ apo-BFR

Absorption change measured at 340 nm as a function of time after the addition of 400 iron (II) ions per apo-protein molecule. The proteins were in 100 mM Mes buffer, pH 6.5, at a concentration of 0.5 μM. Temperature was 30 °C, pathlength 1 cm. Inset is the initial 20 s of the reaction, showing in greater detail phase 2 oxidation.

previous studies [21]. Fitting of the change of absorbance at 425 nm measured at 20 °C for the addition of 100 Fe (II) ions per BFR molecule to a first-order process yielded a rate of $28 \pm 3\ s^{-1}$. Two of the dinuclear-iron site variants, $E^{18} \rightarrow A$ apo-BFR and $E^{51} \rightarrow A$ apo-BFR, displayed an enhanced rate of their haem perturbation under similar conditions ($90 \pm 10\ s^{-1}$). $E^{94} \rightarrow A$ apo-BFR, the other dinuclear-iron site variant, exhibited a haem perturbation rate very similar to that of wild-type apo-BFR at 20 °C ($25 \pm 2\ s^{-1}$), but at 30 °C the rate was significantly faster than for wild-type apo-BFR ($70 \pm 5\ s^{-1}$ compared with $140 \pm 20\ s^{-1}$). The perturbation amplitude per haem in each of the dinuclear-iron site variants was significantly reduced compared with that of wild type, and in the case of $E^{51} \rightarrow A$ apo-BFR, the sign of the absorbance change was inverted. The haem perturbation rate of the 3-fold channel variant, $D^{118} \rightarrow A$ apo-BFR, was slightly less than that of wild-type apo-BFR both at 20 °C and 30 °C ($20 \pm 3\ s^{-1}$ and $45 \pm 3\ s^{-1}$ respectively), while the amplitude of the perturbation, corrected to account for the slightly lower haem loading of the 3-fold channel variant, was found to be only marginally reduced.

In order to account for the differences in phase 1 observed between the BFR variants and wild-type BFR, the origin of the shift in the haem Soret absorption should be considered. The effect could arise either from a direct electrostatic interaction of positively charged metal ions with the haem system or from a protein conformational change detected at the haem consequent upon the binding of iron (II) ions. The three dinuclear-iron site variants exhibited significant changes in the rate and amplitude of their phase 1 haem perturbations whereas the 3-fold channel variant did not, indicating that iron (II) binds at the proposed dinuclear-iron site. In each of the dinuclear-iron site variants, the rate (at least at 30 °C) is increased and the amplitude is reduced. Variant $E^{51} \rightarrow A$ BFR gave rise to a perturbation opposite in sign to that of wild-type BFR. That this variant should give rise to the most significant difference in the perturbation was not unexpected, since E^{51} is next to the haem-ligating M^{52} residue in the BFR polypeptide.

Phases 2 and 3 of iron uptake by wild-type apo-BFR and its variants were investigated by the addition of ferrous ammonium sulphate to aerobic solutions of the proteins, and the subsequent measurement of absorption at 340 nm as a function of time. Figure 3(a) shows a comparison of absorption increases at 340 nm observed after the addition of 400 iron (II) ions per protein molecule to wild-type apo-BFR and its three dinuclear-iron site variants. Phase 2, which is complete in the wild-type protein (under these experimental conditions) within about 10 s of the addition of ferrous ions, is shown more clearly in Figure 3(b). In $E^{18} \rightarrow A$, $E^{51} \rightarrow A$ and $E^{94} \rightarrow A$ apo-BFRs, phase 2 is much less well resolved from phase 3 than in wild-type BFR, and both phases occur over a much increased time course. Clearly, oxidation proceeds at a greatly reduced rate in each of the dinuclear-iron site variants. A similar comparison of absorption at 340 nm after the addition of 400 iron (II) ions per protein molecule between wild-type apo-BFR and the 3-fold channel variant $D^{118} \rightarrow A$ apo-BFR is shown in Figure 4. The inset shows the initial 20 s of the reaction. Phases 2 and 3 in $D^{118} \rightarrow A$ BFR proceed at a slightly reduced rate compared with wild-type BFR.

From these data it is evident that the presence of the dinuclear-iron site residues E^{18}, E^{51} and E^{94} is essential for iron (II) oxidation to occur at the rate observed in the wild-type protein, whereas for the 3-fold channel residue D^{118} this is not so. Thus it can be concluded that the site proposed to form a dinuclear-iron centre in the BFR subunit has key importance for the

Table 2 Summary of the data presented here

Abbreviation used: N/A, not applicable.

Sample	Phase 1 (haem perturbation) measured at 425 nm after the addition of 100 iron (II) or zinc (II) ions per BFR molecule			Phase 2 measured at 340 nm	Phase 3* (core formation) measured at 340 nm	Comments
	Concentration of 24-mer after mixing (μM)	Rate of haem perturbation at 425 nm, 20 °C (s^{-1})†	Amplitude of haem perturbation (A_{425})‡			
Wild-type BFR Addition of iron (II)	2.25	28 ± 3	~ -0.025	Rate§ of 0.48 ± 0.05 s^{-1}	Complete within 40 min of addition of iron (II) ions	See [21]
$E^{18} \rightarrow A$ BFR Addition of iron (II)	2.5	90 ± 10	~ -0.011	Much slower	Much slower	Substitution has greatest effect on the ability of BFR to catalyse iron (II) oxidation
$E^{51} \rightarrow A$ BFR Addition of iron (II)	1.25	90 ± 10	$\sim +0.005$	Much slower	Much slower	Substitution has a significant effect on iron (II) oxidation
$E^{94} \rightarrow A$ BFR Addition of iron (II)	2.25	25 ± 2¶	~ -0.004	Much slower	Much slower	Similar to $E^{51} \rightarrow A$ BFR in its effect on iron (II) oxidation
$D^{118} \rightarrow A$ BFR Addition of iron (II)	2.5	20 ± 3**	~ -0.023	Rate§ of 0.35 ± 0.05 s^{-1}	Slightly slower	Not significantly different from wild type
Wild-type BFR Addition of zinc (II)	2.5	~ 230	~ -0.023	N/A	N/A	Indicates binding of zinc (II) ions at the ferroxidase centre
Wild-type BFR containing 48 zinc (II) ions per 24-mer	0.5	Not measured	Not measured	Not observed	Extremely slow	Iron oxidation rate similar to that of protein-free auto-oxidation

* Measured using a conventional spectrophotometer for the addition of 400 iron (II) ions per 24-mer. BFR concentration was 0.5 μM, temperature 30 °C.
† Rate calculated by fitting measurement to first-order process.
‡ Amplitude corrected, relative to wild-type BFR, for differences in haem loading.
§ Measured by stopped flow at 30 °C for the addition of 400 iron (II) ions per 24-mer. Concentration of BFR was approximately 0.5 μM after mixing.
¶ At 30 °C wild-type BFR exhibits a rate of 70 ± 5 s^{-1} at 425 nm, while that measured for $E^{94} \rightarrow A$ is 140 ± 20 s^{-1}.
** At 30 °C $D^{118} \rightarrow A$ exhibits a rate of 45 ± 3 s^{-1}.

ferroxidase activity of the protein and can thus be identified as the ferroxidase centre. The 3-fold channel residue D^{118} has no major role in the mechanism of oxidation.

The overall changes in absorbance at 340 nm for wild-type BFR and its variants are approximately equal, indicating that iron (II) oxidation reaches completion in all of the samples. This is perhaps unsurprising, because it is known that even in ferritins that lack a ferroxidase centre, for example L-chain homopolymer [25], iron (II) oxidation is still observed and an iron core formed. The rate at which oxidation proceeds in such proteins, however, is significantly less than in those containing ferroxidase centres. This indicates that iron (II) oxidation in ferritins can occur by different mechanisms [38]. Thus mutation of the ferroxidase centre of BFR slows the most rapid oxidation pathway, but other oxidation pathways are clearly unaffected, and consequently oxidation is still observed.

We note that oxidation of iron (II) by O_2 in aqueous solution in the absence of protein proceeds at a rate dependent upon pH, being faster at higher pH. Provided that iron (II) and O_2 can reach the BFR cavity then oxidation and precipitation will proceed. Furthermore, if the inner surface of the protein provides sites of iron (III) binding that facilitate nucleation for iron precipitation, then the core formation will be further speeded up compared with the same process in the absence of protein. The importance of the present work is the demonstration that there is rapid formation of a dinuclear iron (II) centre at the site identified crystallographically, that these iron (II) ions are rapidly oxidized by O_2, and further that this process is crucial to obtain core formation at the same rate as in the wild-type protein. A summary of data presented here is given in Table 2.

The inhibition of iron (II) oxidation at the ferroxidase centre by zinc (II) ions

It might be anticipated that a non-redox active but tightly binding bivalent metal ion, such as zinc (II), would also be rapidly taken up by the ferroxidase centre in competition with iron (II), thus preventing the subsequent steps of oxidation. Therefore, the effect of zinc (II) ions on the ability of wild-type apo-BFR to catalyse the oxidation of iron (II) to iron (III) was investigated. The addition of 48 zinc (II) ions per apo-BFR molecule followed by 400 iron (II) ions per molecule resulted in the 340 nm absorption trace shown in Figure 5. Equivalent measurements in both the absence of zinc (II) and the absence of zinc (II) and BFR are also presented. The presence of zinc (II) resulted in a considerable reduction in the overall rate of iron (II) oxidation, phase 2 of iron uptake not being observed. Stopped-flow measurements of changes of absorption in the Soret region

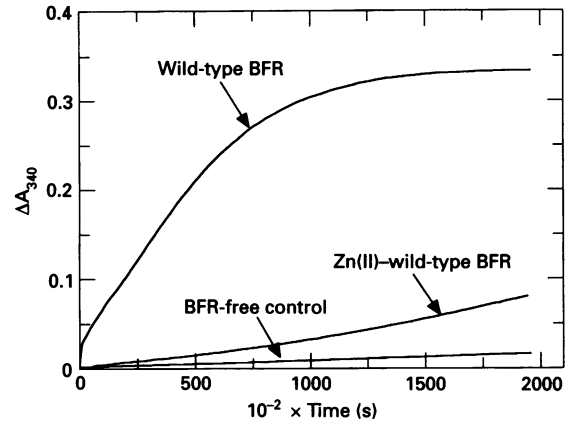

Figure 5 Inhibition by zinc (II) ions of wild-type BFR-catalysed iron (II) oxidation

Absorption change measured at 340 nm as a function of time for the addition of: 400 iron (II) ions per molecule to a sample of wild-type apo-BFR; 400 iron (II) ions per BFR molecule to a sample of wild-type BFR containing 48 zinc (II) ions per molecule; and a comparable amount of iron (II) ions to 100 mM Mes buffer, pH 6.5. Proteins were at a concentration of 0.5 μM in 100 mM Mes buffer, pH 6.5. Temperature was 30 °C, pathlength 1 cm.

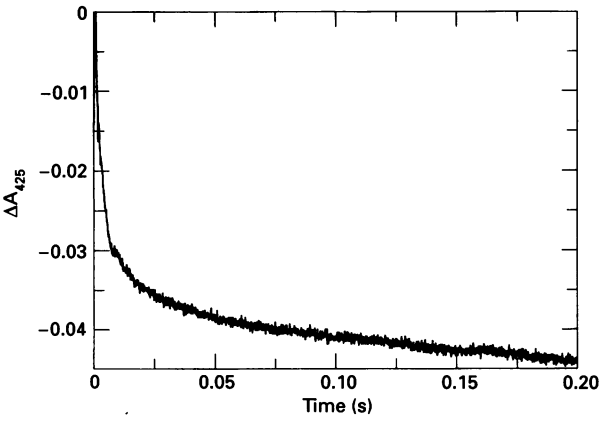

Figure 6 Detection of a haem perturbation in wild-type apo-BFR following the addition of zinc (II) ions

Absorption change at 425 nm measured by the stopped-flow method as a function of time after the addition of 50 zinc (II) ions per apo-BFR molecule. The protein (concentration after mixing, 2.5 μM) was in 100 mM Mes buffer, pH 6.5. Temperature was 20 °C, pathlength 1 cm.

(405–425 nm) indicated that the addition of 50 zinc (II) ions per BFR molecule causes a perturbation of the haem Soret band. The measurement at 425 nm is presented in Figure 6. The amplitude of the absorption change resulting from the addition of zinc (II) ions to apo-BFR was similar to that observed for the addition of iron (II) ions under the same conditions, but the rate of the perturbation was found to be about an order of magnitude greater. For 100 zinc (II) ions per apo-BFR, the rate was found to be $\sim 230\ s^{-1}$ at 20 °C compared with $\sim 28\ s^{-1}$ for 100 iron (II) ions per apo-BFR at 20 °C. In addition to the very rapid decrease of absorption at 425 nm, complete within 50 ms under these experimental conditions, the trace contains a second, slower component associated with a much smaller amplitude. The origin of the second component is not known, but investigation of its wavelength dependence (results not shown) revealed that it is observed at low amplitudes over a wide range of wavelengths, and is not thought to be associated with the haem perturbation phase of metal ion uptake.

Consistent with the finding of a significantly faster haem perturbation phase after the addition of zinc (II) ions to apo-BFR [compared with iron (II)] was the observation that after the addition of 100 ions per molecule of wild-type apo-BFR of both zinc (II) and iron (II) (in a 1:1 mixture), ferroxidase activity was not detected (results not shown). This indicates that zinc (II) ions bind the ferroxidase centre in preference to iron (II).

The present work demonstrates that zinc (II) is able to bind at the ferroxidase centre with a higher affinity than iron (II). The affinity difference is not a surprise, since the Irving Williams series indicates that zinc (II) generally has tighter binding properties than does high-spin iron (II). Zinc (II) binding appears to abolish phase 2 oxidation and severely slows the rate of phase 3 oxidation. A summary of experimental data is presented in Table 2.

Mechanism of iron uptake by BFR

The present work establishes clearly that the dinuclear-metal site first proposed by us and latterly identified by X-ray crystallography is the site that can bind a pair of iron (II) ions and catalyse reduction of dioxygen. This process is required for the rapid formation of an iron core in apo-BFR. Together with previous kinetic and spectroscopic studies, it is apparent that apo-BFR rapidly binds two iron (II) ions per ferroxidase centre, and in the presence of oxygen, this is followed by the oxidation of both iron (II) ions to iron (III) ions. Zinc (II) ions are potent inhibitors of iron (II) uptake into this centre, and hence of ferroxidase centre oxidation. The mechanism of inhibition appears to be through a higher affinity of zinc (II) ions for the ferroxidase centre as is also observed in both native H/L heteropolymers and H-chain ferritins at relatively low zinc (II)/ferritin ratios [18,39,40]. Under these conditions zinc (II) is a competitive inhibitor of iron (II) binding, although at higher zinc (II)/ferritin ratios other sites in the protein may become occupied [41]. Inhibition of iron (II) uptake also leads to inhibition of core formation in BFR.

The mechanism of iron loading after oxidation of the two irons is still unclear, and the present work does not seek to address this question. However, two limiting models can be considered. In the first the centre can be viewed as a catalytic site of dioxygen reduction and iron (II) oxidation, in which, once formed, a pair of iron (II) ions remain bound with no exchange. The iron (II) ions that form the core must in this case travel by a different route to the centre. In the second model, the ferroxidase centre is the catalytic site of O_2 reduction but is also on the pathway of metal ions into the core, acting as a metal-ion shuttle, constantly emptying of iron (III) and refilling with iron (II). The observations, described here and in previous reports, that bear upon this question are as follows. (1) The phase 2 fast oxidation process is observed only on reaction of iron (II) with apo-BFR or BFR containing less than 48 irons per molecule. Even after treatment of apo-BFR with 48 iron (II) ions, followed by oxidation and a delay of 22 h, phase 2 is not detected upon addition of further iron (II) ions [21]. (2) Addition of up to 48 iron (II) ions per BFR in the presence of O_2 gives two phases, 1 and 2, only. Only when more than 48 iron (II) ions have been added to the protein does core formation appear to begin [21]. (3) Alterations of the ferroxidase centre by site-directed mutagenesis affect the rates of all three phases of iron uptake (this work). (4)

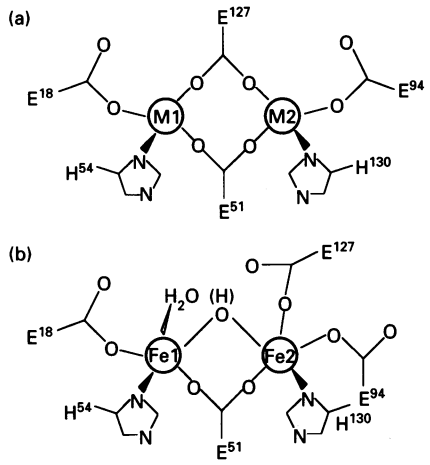

Figure 7 Schematic representations of the dinuclear-metal site of BFR

(**a**) The site identified in the crystal structure of *E. coli* BFR by Frolow et al. [9]. M1 and M2 are the metal centres 1 and 2 respectively. (**b**) Possible structure of the dinuclear site following oxidation of the two Fe(II) ions to Fe(III) ions.

EPR spectra recorded 2 min after oxidation of the ferroxidase centre show the presence of mononuclear high-spin iron (III) in appreciable amounts, even after the addition of between 24 and 48 iron (II) ions [21].

One possible interpretation of these observations is that the dinuclear-iron species forms at the ferroxidase centre when iron (II) and O_2 are added to the apo-protein and, once formed, does not exchange any iron with the core or the surroundings. However, the EPR signals cannot arise from a μ-oxo bridged pair of iron (III) ions and are unlikely to arise from a pair of iron (III) ions situated ~ 4 Å apart, especially if a carboxylate bridge is present between them. Hence the EPR experiments suggest that the dinuclear-iron species at the ferroxidase centre breaks up and loses iron (III) to a further site within the protein and becomes EPR detectable.

In our previous report [21] we suggested that the site of iron (II) oxidation in BFR may switch from the ferroxidase centre to the surface of the growing core crystallite, as is thought to occur in core formation by mammalian ferritins [15,38]. In such a mechanism, the role of the ferroxidase centre would be to initiate core nucleation. The effect of the ferroxidase centre mutagenesis on phase 3 oxidation is clearly seen from Figures 3(a) and 3(b). This effect may arise either because the ferroxidase centre is directly involved in all stages of core formation, or because the altered ferroxidase centres are unable to initiate the nucleation of a core of the size and/or structure necessary to enable it to act as an efficient site of iron (II) oxidation. Thus a role for the BFR ferroxidase centre in initiating core formation only, with the core then taking over as the main oxidation site, is not excluded by our work.

Structure of the ferroxidase centre of BFR and comparison with other dinuclear-iron centres

The crystal structure of *E. coli* BFR showed the presence of two electron-dense peaks from a dinuclear metal site within each α-helical bundle [9]. The ligands to the pair of metal ions were E^{18}, E^{51}, H^{54}, E^{94}, E^{127} and H^{130} (see Figure 7a), though the chemical nature and redox states of the two metal ions were not identified. The model of the dinuclear metal centre is very similar to that originally proposed on the basis of molecular modelling studies [8].

The amino acid sequences and secondary structures of BFR and two other structurally characterized proteins that contain a catalytically active dinuclear-iron centre, namely ribonucleotide reductase (RNR) and methane mono-oxygenase (MMO), each share common features associated with the dinuclear site [8,42,43]. All contain a four-α-helical bundle with similar dinuclear-iron centre connectivities, as shown in Figure 8. The location on the α-helices of the dinuclear metal ligands and the relative spacings between them are remarkably similar for all three proteins. In the terminology proposed by Fox et al. [44], RNR and MMO are class II di-iron-oxo proteins, and BFR is also a class II di-iron protein.

Three structures of the dinuclear-iron-containing component of RNR (the R2 subunit) have been determined, one in which the

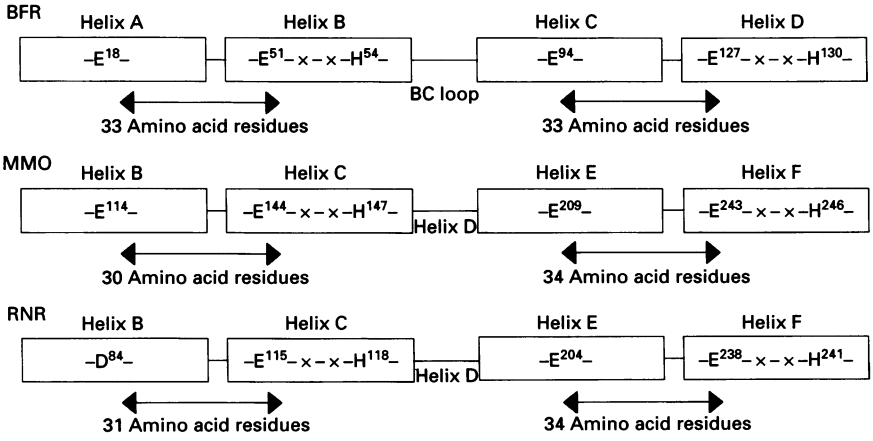

Figure 8 Amino acid sequence comparison of BFR with MMO and RNR

Amino acid sequence comparison of BFR with the two structurally characterized dinuclear-iron containing proteins, MMO and RNR [42,43,47,48]. Only residues that serve as metal-ion ligands are indicated. The α-helices that form the four-α-helical bundle of each protein subunit are schematically represented by boxes.

dinuclear site is devoid of metal ions [45], one containing a pair of bivalent manganese ions [46] and one with two ferric ions [42]. The three structures show that the exact positions of the functional groups that are actual or potential metal ligands depend upon the presence or absence of metal ions, and upon the oxidation states or charges of the metal ions, although there are no major structural differences in the protein. The apo-protein, with a cluster of four carboxylate residues, probably contains four protons at the metal binding site. The structure of the site containing two manganese (II) ions has two carboxylate bridges (E^{115} and E^{238}) and no μ-oxo or μ-hydroxo bridge, yielding a site that is apparently charge neutral. The site containing two iron (III) ions gains one bridging O^{2-} group and loses one bridging carboxylate (E^{238}) so that the metal ion pair is asymmetrical, but again the site is neutral.

The ferroxidase centre structure of BFR given by Frolow et al. [9] appears to be identical to that of the $Mn(II)_2$ centre in RNR, and hence is also charge neutral. Since the BFR protein analysed by Frolow et al. [9] was crystallized by addition of manganese (II) ions, it is probable that the dinuclear centre observed by these workers contains a pair of manganese (II) ions. Indeed, we have recently demonstrated, by EPR spectroscopy, the binding of two manganese (II) ions to each BFR subunit (A. M. Keech, N. E. Le Brun, S. C. Andrews, J. R. Guest, G. R. Moore and A. J. Thomson, unpublished work). Furthermore, the comparison with the RNR structural data suggests that the diferric form of the dinuclear site in BFR is likely to be different from the structure given by Frolow et al. [9] (see for example Figure 7b). One indication that the two iron (III) ions may become inequivalent after oxidation comes from the significantly different rates of core formation observed in the BFR variants $E^{18} \rightarrow A$ and $E^{94} \rightarrow A$ (see Figure 3). In the BFR structure reported by Frolow et al. [9] E^{18} and E^{94} (ligands of M1 and M2 respectively) are virtually equivalent, being related by an approximate 2-fold axis of symmetry. If these residues remain equivalent after oxidation, it might be expected that replacing each of these residues would produce equivalent reductions in the rate of core formation.

We thank the BBSRC and the Wellcome Trust for supporting our work on bacterioferritin, and the Biomolecular Sciences Committee of the BBSRC and EPSRC for its support of the UEA Centre for Metalloprotein Spectroscopy and Biology. N.L.B. thanks the Wellcome Trust for the award of a Prize Fellowship, and S.C.A. thanks the BBSRC for the award of an Advanced Fellowship.

REFERENCES

1 Andrews, S. C., Smith, J. M. A., Guest, J. R. and Harrison, P. M. (1989) Biochem. Biophys. Res. Commun. **158**, 489–496
2 Andrews, S. C., Harrison, P. M. and Guest, J. R. (1989) J. Bacteriol. **171**, 3940–3947
3 Ford, G. C., Harrison, P. M., Rice, D. W., Smith, J. M. A., Treffry, A. and Yariv, J. (1984) Philos. Trans. R. Soc. London B Biol. Sci. **304**, 551–565
4 Andrews, S. C., Smith, J. M. A., Yewdall, S. J., Guest, J. R. and Harrison, P. M. (1991) FEBS Lett. **293**, 164–168
5 Andrews, S. C., Findlay, J. B. C., Guest, J. R., Harrison, P. M., Keen, J. N. and Smith, J. M. A. (1991) Biochim. Biophys. Acta **1078**, 111–116
6 Andrews, S. C., Arosio, P., Bottke, W. et al. (1992) J. Inorg. Biochem. **47**, 161–174
7 Grossman, M. J., Hinton, S. M., Minak-Bernero, V., Slaugther, C. and Stiefel, E. I. (1992) Proc. Natl. Acad. Sci. U.S.A. **89**, 2419–2423
8 Cheesman, M. R., Le Brun, N. E., Kadir, F. H. A. et al. (1993) Biochem. J. **292**, 47–56
9 Frolow, F., Kalb, A. J. and Yariv, J. (1994) Struct. Biol. **1**, 453–460
10 Hudson, A. J., Andrews, S. C., Hawkins, C. et al. (1993) Eur. J. Biochem. **218**, 985–995
11 Cheesman, M. R., Thomson, A. J., Greenwood, C., Moore, G. R. and Kadir, F. (1990) Nature (London) **346**, 771–773
12 Andrews, S. C., Le Brun, N. E., Barynin, V. et al. (1995) J. Biol. Chem., in the press
13 Watt, G. D., Frankel, R. B., Papaefthymiou, G. C., Spartalian, K. and Stiefel, E. I. (1986) Biochemistry **25**, 4330–4336
14 St. Pierre, T. G., Webb, J. and Mann, S. (1989) in Biomineralisation (Mann, S., Webb, J. and Williams, R. J. P., eds.), pp. 295–344, VCH, Weinheim
15 Macara, I., Hoy, T. G. and Harrison, P. M. (1972) Biochem. J. **126**, 151–162
16 Bryce, C. F. A. and Crichton, R. R. (1973) Biochem. J. **133**, 301–309
17 Lawson, D. M., Treffry, A., Artymuik, P. J. et al. (1989) FEBS Lett. **254**, 207–210
18 Bauminger, E. R., Harrison, P. M., Hechel, D., Nowik, I. and Treffry, A. (1991) Biochim. Biophys. Acta **1118**, 48–58
19 Bauminger, E. R., Harrison, P. M., Hechel, D. et al. (1993) Biochem. J. **296**, 709–719
20 Sun, S. and Chasteen, N. D. (1992) J. Biol. Chem. **267**, 25160–25166
21 Le Brun, N .E., Wilson, M. T., Andrews, S. C. et al. (1993) FEBS Lett. **333**, 197–202
22 Levi, S., Luzzago, A., Cesareni, G. et al. (1988) J. Biol. Chem. **263**, 18086–18092
23 Bauminger, E. R., Treffry, A., Hudson, A. J. et al. (1994) Biochem. J. **302**, 813–820
24 Waldo, G. S., Ling, J. S., Sanders-Loehr, J. and Theil, E. C. (1993) Science **259**, 796–798
25 Levi, S., Salfeld, J., Franceschinelli, F., Cozzi, A., Dorner, M. H. and Arosio, P. (1989) Biochemistry **28**, 5179–5184
26 Lawson, D. M., Artymuik, P. J., Yewdall, S. J. et al. (1991) Nature (London) **349**, 541–544
27 Treffry, A., Hirzmann, J., Yewdall, S. J. and Harrison, P. M. (1992) FEBS Lett. **302**, 109–112
28 Kunkel, T. A. (1985) Proc. Natl. Acad. Sci. U.S.A. **82**, 488–492
29 Tabor, S. and Richardson, C. C. (1987) Proc. Natl. Acad. Sci. U.S.A. **84**, 4767–4771
30 Sanger, F., Coulson, A. R., Barrell, B. G., Smith, A. J. H. and Roe, B. A. (1980) J. Mol. Biol. **143**, 161–178
31 Andrews, S. C., Smith, J. M. A., Hawkins, C., Williams, J. M., Harrison, P. M. and Guest, J. R. (1993) Eur. J. Biochem. **213**, 329–338
32 Messing, J. (1983) Methods Enzymol. **101**, 20–78
33 Drysdale, J. W. and Munro, H. N. (1965) Biochem. J. **95**, 851–857
34 Smith, P. K., Krohn, R. I., Hermanson, G. T. et al. (1985) Anal. Biochem. **150**, 76–85
35 Falk, J. E. (1964) in Porphyrins and Metalloporphyrins, pp. 181–182, BBA Library vol. 2, Elsevier, North Holland
36 Le Brun, N. E., Cheesman, M. R., Thomson, A. J. et al. (1993) FEBS Lett. **323**, 261–266
37 Bauminger, E. R., Cohen, S. G., Dickson, D. P. E., Levy, A., Ofer, S. and Yariv, J. (1980) Biochim. Biophys. Acta **623**, 237–242
38 Crichton, R. R. and Charloteaux-Wauters, M. (1987) Eur. J. Biochem. **164**, 485–506
39 Macara, I. G., Hoy, T. G. and Harrison, P. M. (1973) Biochem. J. **135**, 785–789
40 Sun, S., Arosio, P., Levi, S. and Chasteen, N. D. (1993) Biochemistry **32**, 9362–9369
41 Yablonski, M. J. and Theil, E. C. (1992) Biochemistry **31**, 9680–9684
42 Nordlund, P., Sjoberg, B.-M. and Eklund, H. (1990) Nature (London) **345**, 593–598
43 Rosenzweig, A. C., Frederick, C. A., Lippard, S. J. and Nordlund, P. (1993) Nature (London) **366**, 537–543
44 Fox, B. G., Shanklin, J., Ai, J., Loehr, T. M. and Sanders-Loehr, J. (1994) Biochemistry **33**, 12776–12786
45 Aberg, A., Nordlund, P. and Eklund, H. (1993) Nature (London) **361**, 276–278
46 Atta, M., Nordlund, P., Aberg, A., Eklund, H. and Fontecave, M. (1992) J. Biol. Chem. **267**, 20682–20688
47 Stainthorpe, A. C., Lees, V., Salmond, G. P. C., Dalton, H., and Murrel, J. C. (1990) Gene **91**, 27–34
48 Nordlund, P., Dalton, H. and Eklund, H. (1992) FEBS Lett. **307**, 257–262

Received 7 April 1995/12 July 1995; accepted 25 July 1995